Chaotic dynamics in a three-dimensional superconducting microwave billiard

H. Alt,[1] H.-D. Gräf,[1] R. Hofferbert,[1] C. Rangacharyulu,[2] H. Rehfeld,[1] A. Richter,[1] P. Schardt,[1,*] and A. Wirzba[1]
[1]*Institut für Kernphysik, Technische Hochschule Darmstadt, D-64289 Darmstadt, Germany*
[2]*Department of Physics, University of Saskatchewan, Saskatoon, Saskatchewan, Canada S7N OWO*
(Received 10 October 1995; revised manuscript received 22 March 1996)

We present measurements on a superconducting *three-dimensional*, partly chaotic microwave billiard shaped such as a small deformed cup. We analyze the statistical properties of the measured spectrum in terms of several methods originally derived for quantum systems such as eigenvalue statistics and periodic orbits and obtain, according to a model of Berry and Robnik [J. Phys. A **17**, 2413 (1984)], a mixing parameter of about 25%. In numerical simulations of the classical motion in the cup, the degree of chaoticity has been estimated. This leads to an invariant chaotic Liouville measure of about 45%. The difference between this figure and the mixing parameter is due to the limited accuracy of the statistical analysis, caused by both the fairly small number of 286 resonances and the rather poor desymmetrization of the microwave cavity. Concerning the periodic orbits of the classical system, we present a comparison with the length spectrum of the resonator and introduce a bouncing ball formula for electromagnetic billiards. [S1063-651X(96)06008-4]

PACS number(s): 05.45.+b, 41.20.Bt, 41.20.Jb

I. INTRODUCTION

In the past few decades the theoretical investigation of two-dimensional Euclidian and Riemannian geometries, so-called billiards, has led to a very fruitful discipline in nonlinear physics [1–3]. Due to the conserved energy of the ideal particle propagating inside the billiard's boundaries with specular reflections on the walls, the plain billiard belongs to the class of Hamiltonian systems with the lowest degree of freedom in which chaos can occur, which depends only on the given boundary shape. Because of their simplicity, two-dimensional billiards are in particular adequate to study the behavior of the particle in the corresponding quantum regime [4–6] where spectral properties are completely described by the stationary Schrödinger equation

$$H\Psi(\vec{r}) = -\frac{\hbar^2}{2m}\Delta\Psi(\vec{r}) = E\Psi(\vec{r}) \tag{1}$$

inside the domain $\mathcal{G}$ with Dirichlet boundary conditions on the walls

$$\Psi(\vec{r})|_{\partial\mathcal{G}} = 0. \tag{2}$$

In this context the investigation of quantum chaos has become one of the most fascinating goals of theoretical physics at the end of this century [7,8].

About five years ago experimentalists even found very effective techniques to simulate the quantum billiard problem with the help of macroscopic devices. Due to the equivalence of the stationary Schrödinger equation and the classical Helmholtz equation in two dimensions one is able to model the billiard by a similarly shaped electromagnetic cavity [9–11]. In former publications we have demonstrated the high accuracy of large ensembles of measured eigenvalues as well as of resonance shapes and the attached widths in *superconducting* cavities formed such as desymmetrized Bunimovich and truncated Hyperbola billiards [12–15].

Especially the statistical analysis of measured (or numerically simulated) eigenvalue sequences confirms that a distinction between classical chaotic and regular systems from the quantum point of view is only possible in the semiclassical regime (formally spoken for $\hbar \to 0$), where the particle's de Broglie wavelength is sensitive to details of the billiard's borderline. One of the most surprising and primarily empirical results of these investigations is the fact that quantum spectra of classical chaotic Hamiltonian systems can be described in a universal manner that depends only on the global symmetry of the underlying dynamics: The quantum pendants of time-reversal invariant classically chaotic systems typically reveal spectral structures that are reproduced excellently by statistical properties of the Gaussian orthogonal ensemble (GOE) of random matrix theory [16–18]. On the other hand, classically regular systems usually lead to spectral fluctuations on the wave dynamical side according to uncorrelated Poissonlike distributed random numbers [19].

In this article we present investigations that were performed on a three-dimensional superconducting billiard. Due to the polarization properties of the electromagnetic fields $\vec{E}$ and $\vec{B}$ inside the cavity the full vectorial Helmholtz equations [20]

$$\left(\Delta + \epsilon\mu\frac{\omega^2}{c_0^2}\right)\vec{E}(\vec{r}) = \vec{0}, \tag{3}$$

$$\left(\Delta + \epsilon\mu\frac{\omega^2}{c_0^2}\right)\vec{B}(\vec{r}) = \vec{0} \tag{4}$$

have to be used with corresponding boundary conditions

$$\vec{E}_{\parallel}(\vec{r})|_{\partial\mathcal{G}} = \vec{0}, \quad \vec{B}_{\perp}(\vec{r})|_{\partial\mathcal{G}} = \vec{0} \tag{5}$$

on the walls, which are assumed to be ideally conducting. Of course, the analogy with the corresponding scalar Schrö-

*Present address: Siemens AG, Bereich Medizinische Technik, D-91052 Erlangen, Germany.

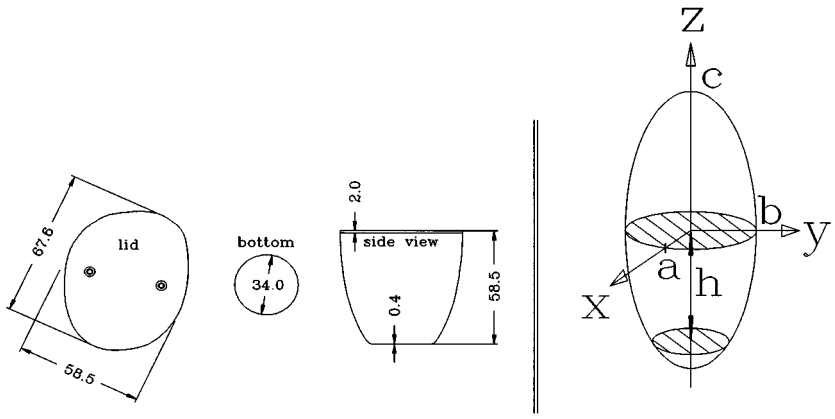

FIG. 1. Geometry of the 3D cup. The investigated microwave resonator, together with its measures (in millimeters), is given on the left-hand side. The model of the barrel billiard that was used for several numerical simulations is shown on the right-hand side. The latter has been constructed from one-half of a three-axial ellipsoid cut with an additional plane at distance h from the origin.

dinger equation in the same geometry is fully lost. Instead of talking of the semiclassical limit we have to describe the classical electromagnetic billiard in this region in terms of ray-optical characteristics, where features of the periodic orbits inside the geometry dominate the corresponding wave optical side.

Three-dimensional systems have so far only scarcely been investigated experimentally. To our knowledge, the first experiments with electromagnetic waves in cavities simulating acoustic wave phenomena in rooms were performed by Schröder [21]. Acoustic model statistics in metal blocks have also been investigated [22,23]. Very recently statistical properties of eigenfrequency distributions in asymmetrically shaped microwave cavities have been reported [24]. Theoretically quantum effects, as well as their electromagnetic counterparts in three-dimensional systems, were treated in Refs. [25–27].

II. EXPERIMENT

We have investigated a small deformed three-dimensional (3D) cavity made from an open, deep drawn niobium cup with a welded lid to cover it. Before welding the two parts together, the cup was deformed at its open end to destroy its rotational symmetry. Its measures are given in Fig. 1. The total volume of the resonator was determined by filling it with water and measuring the additional weight, yielding a volume of $122.5 \pm 1.9\ \mathrm{cm}^3$. The shape of the cup can be approximated by cutting a three-axial ellipsoid twice perpendicular to its main axis (see also Fig. 1) and then deforming it slightly. The microwaves were transmitted into and out of the cavity by two small antennas in the lid. The whole resonator was cooled down in helium atmosphere at a temperature of 2 K and a pressure of 38 mbar in one of the cryostats of the superconducting Darmstadt electron linear accelerator S-DALINAC [28] together with the accelerating structures. With this setup we have measured microwave spectra in transmission (antenna 1 for input and antenna 2 for output) as well as in reflection (same antenna for excitation and detection) using a Hewlett Packard network analyzer (model HP8510B) in a frequency range between 0 and 20 GHz, respectively.

Spectra were taken in 10-kHz steps and Fig. 2 shows an extraction of the transmission spectrum between 15 and 20 GHz where typical Q values of up to 10^5 and signal-to-noise ratios of up to 50 dB were obtained. By comparing the three measured spectra 286 resonances could be consistently identified, which form the basis of all following investigations.

For an analysis of this set, however, one has to take into account the following point: Since the geometry of the cup is very close to one that possesses two symmetry planes (xz and yz planes, see Fig. 1), the given set of resonances in the analysis is always compared to a superposition of four independent subspectra.

III. RESULTS AND DISCUSSION

A. Density of eigenmodes

In order to derive meaningful statistical measures for the given eigenvalue sequence it is first necessary to extract the smooth part of the resonator's density of eigenmodes, which is given by the generalized electromagnetic Weyl formula [29–32]

$$\rho^{\mathrm{smooth}}(f) = \frac{8\pi}{c_0^3}|\mathcal{G}|f^2 + \mathrm{const}, \tag{6}$$

where $|\mathcal{G}|$ denotes the volume of the cavity and f the upper

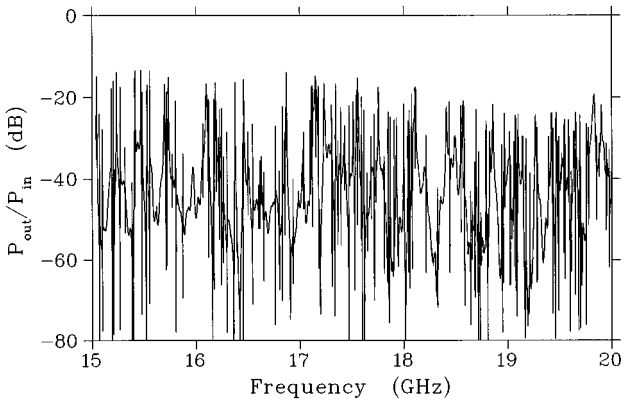

FIG. 2. Measured transmission spectrum in a range between 15 and 20 GHz. The ordinate shows the ratio of the output power relative to the input power on a logarithmic scale. As can be seen from the figure, the eigenfrequencies appear as sharp peaks with a Q value of up to 10^5 and a signal-to-noise ratio of up to 50 dB.

frequency limit of the given spectrum. The constant term contains contributions of the surface's curvature as well as of the edges of the cavity. The total density of eigenmodes contains, in addition, a fluctuating part

$$\rho(f)=\rho^{\mathrm{smooth}}(f)+\rho^{\mathrm{fluc}}(f)=\sum_i \delta(f-f_i), \tag{7}$$

where f_i denotes the eigenfrequencies of the resonances.

It is very instructive to compare Eq. (6) with the corresponding expression for the three-dimensional Schrödinger problem in the same geometry, i.e.,

$$\rho^{\mathrm{smooth}}(f)=\frac{4\pi}{c_0^3}|\mathcal{G}|f^2-\frac{\pi}{2c_0^2}|\partial\mathcal{G}|f+\mathrm{const.} \tag{8}$$

Due to the already mentioned polarization features of the modes, the leading term in the electromagnetic formula Eq. (6) is twice the corresponding term in the scalar problem Eq. (8) because of two transverse directions of polarization relative to the axis of propagation. In addition, these two polarizations, which are known as TM and TE modes in certain geometries, provide linear terms in the smoothed eigenmode density of the same magnitude but with different sign. Thus due to cancellation there is no linear contribution in Eq. (6), whereas this term survives in the scalar case and is proportional to the cavity's surface $|\partial\mathcal{G}|$. Even if a clear separation in the attached TM and TE modes is not possible in cases of arbitrary geometries, like in the case of our cup, this linear term vanishes for all piecewise smooth boundaries [31,32]. The constant terms in both Eqs. (6) and (8) are of the same origin, i.e., the curvature of the surface and the edge angles of the cavity.

To determine the spectral fluctuations, the smooth part of the eigenmode density in the measured spectrum had to be eliminated. For this we constructed from Eq. (7) the staircase function

$$N(f)=\int_0^f df'\rho(f')=\sum_i \Theta(f-f_i)=\sum_{\substack{i\\ f>f_i}} 1+\sum_{\substack{i\\ f=f_i}}\frac{1}{2} \tag{9}$$

and obtained its fluctuating part

$$N^{\mathrm{fluc}}(f)=N(f)-N^{\mathrm{smooth}}(f). \tag{10}$$

Since in the case of our billiard there is no analytical form for the edge contribution of the constant term of Eq. (6) we have fitted a third-order polynomial (without the quadratic term) to the experimental staircase function, i.e.,

$$N^{\mathrm{smooth}}(f)=V_1f^3+V_2f+V_3. \tag{11}$$

In Fig. 3 the remaining fluctuating part of the staircase function can be seen to oscillate around zero as expected. The fitted constant V_1 corresponds to a volume of $119.3\pm0.7\ \mathrm{cm}^3$, which is very close to the correct value of $122.5\pm1.9\ \mathrm{cm}^3$. This difference in the leading term corresponds to an uncertainty of 4 resonances in the measured total spectrum [neglecting the linear and constant term in Eq. (11)].

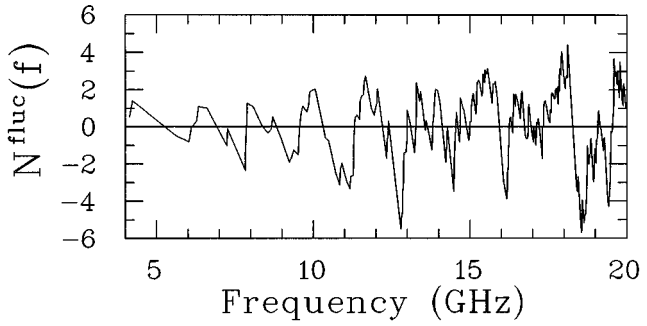

FIG. 3. Remaining fluctuating part of the staircase function after the extraction of the smooth part $N^{\mathrm{smooth}}(f)=V_1f^3+V_2f+V_3$. The particular form of the oscillations around zero indicates that the smooth part was described consistently.

B. Nearest-neighbor spacing distribution

In order to perform a statistical analysis of the given eigenvalue sequence independently from the special size of the resonator, the spectrum was first unfolded, i.e., from the measured sequence of eigenfrequencies $\{f_1,f_2,\ldots,f_i,f_{i+1},\ldots\}$ the spacing $s_i=(f_{i+1}-f_i)/\overline{s}$ between adjacent eigenmodes was obtained by calculating the local average $\overline{s}$ from Eq. (11). The proper normalization of the measured spacings of eigenmodes then yielded the desired nearest-neighbor distribution $P(s)$, i.e., the probability for a certain spacing s.

By comparing $P(s)$ to theoretical expressions one has to take into account, however, that the mechanically only weakly deformed cup (Fig. 1) can, to a good approximation, be constructed of four similar quarter cups, which separately possess the full geometrical information of the object, in which case the measured spectrum would be a superposition of four independent symmetry classes, which are obtained by permuting the boundary conditions on the cutting planes of the quarter cup from electric to magnetic, respectively. Hence one has to be aware of this point in the following statistical analysis of eigenmode spacings.

Furthermore, to obtain a quantitative criterion concerning the degree of chaoticity in the system the spectrum was analyzed in terms of statistical measures from a model of Berry and Robnik [33], which interpolates between the two limiting cases of pure Poissonian and pure GOE behavior for classical regular and chaotic systems, respectively. The final essence of this model is a mixing parameter q, which is directly related to the relative chaotic part of the invariant Liouville measure of the underlying classical phase space in which the motion takes place. According to the herein embedded one-to-one connection between classical phase space and eigenmode density for the two different regions of regular and chaotic motion, a comparison becomes meaningful only for the highly excited domain of the spectrum, which is not sufficiently covered by the frequency range up to 20 GHz investigated here.

In the upper part of Fig. 4 the result for the nearest-neighbor spacing distribution $P(s)$, which describes, as already mentioned, short-range correlations between neighboring unfolded levels, is shown in the form of a histogram. With respect to the superposition of four independent symmetry classes, as noted above, the model of Berry and Rob-

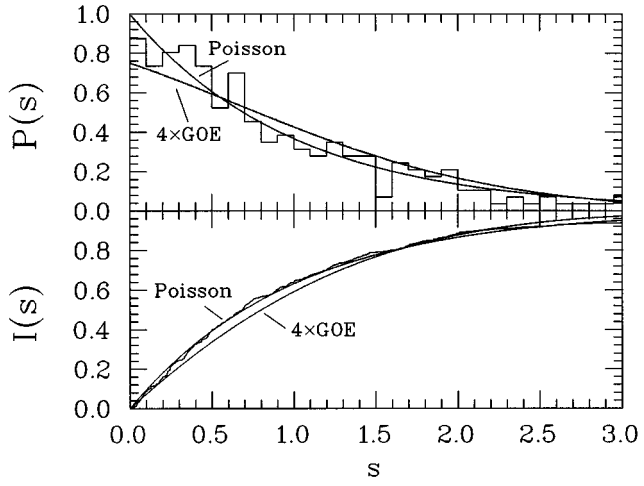

FIG. 4. Ordinary (upper part) and cumulative (lower part) nearest-neighbor spacing distributions for the set of 286 measured eigenfrequencies. In addition to the experimental histograms, the curves for pure Poissonian as well as pure GOE characteristics are shown.

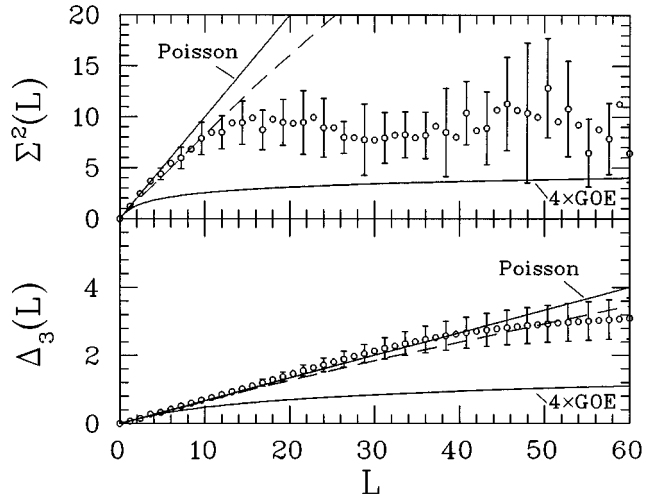

FIG. 5. Number variance Σ^2 and spectral rigidity Δ_3 for the measured spectrum (circles). Again the limiting curves for pure Poissonian and Gaussian distributions are given in the figure. Up to a certain value $L_{\max}$ the Σ^2 curve is well described by a mixing parameter $q \approx 0.30 \pm^{0.20}_{0.30}$ (dashed curve). Above $L_{\max} \approx 10$ the curve shows a clear deviation which is theoretically expected because of the finite set of eigenmodes and the finite lengths of the shortest periodic orbits. The experimental spectral rigidity Δ_3 is only within its error range compatible with the mixing parameter of Σ^2 and possesses a four times larger value of $L_{\max}$, as expected [35]. For a clear representation only every second error bar is shown in the figure.

nik makes the following ansatz for an interpolation between pure Poissonian and pure Gaussian characteristics:

$$P_{4,4}(s,q) = e^{-(1-q)s}\left\{ 16\left(\frac{1-q}{4}\right)^2 \mathrm{erfc}^4\left(\frac{\sqrt{\pi}}{2}\frac{q}{4}s\right) + \left[32\frac{(1-q)}{4}\frac{q}{4} + \frac{\pi}{2}\left(\frac{q}{4}\right)^3 4s \right] \times \exp\left[-\frac{\pi}{4}\left(\frac{q}{4}\right)^2 s^2 \right] \mathrm{erfc}^3\left(\frac{\sqrt{\pi}}{2}\frac{q}{4}s\right) + 12\left(\frac{q}{4}\right)^2 \times \exp\left[-2\frac{\pi}{4}\left(\frac{q}{4}\right)^2 s^2 \right] \mathrm{erfc}^2\left(\frac{\sqrt{\pi}}{2}\frac{q}{4}s\right) \right\}. \quad (12)$$

For inspection the limiting curves of a superposition of four independent pure Poissonians ($q=0$), which again yields one single Poissonian, as well as of four independent GOEs ($q=1$) are also represented in the figure. Note that the superposition results in a clear loss of linear level repulsion for small spacings in the case of pure GOE statistics. Furthermore, there is not much distinction between Poissonian and GOE statistics, anyhow.

It is obvious that $P(s)$ does not allow the determination of the mixing parameter q with reasonable significance, since the fluctuations in the data are larger than the difference between the given smooth curves. To be free of effects due to the binning of $P(s)$ we have also calculated the cumulative nearest-neighbor spacing distribution

$$I(s) = \int_0^s P(s')ds'. \quad (13)$$

The result is presented in Fig. 4 (lower part) together with the curves for the pure distributions, Poisson, and the four superimposed GOE's (labeled 4× GOE). In this case the measured spacings are very close to Poissonian behavior over a large range of s. A fit of $I(s)$ to the data yields $q = 0.16 \pm^{0.25}_{0.16}$ where the uncertainty was determined from analyzing different subsets of the measured data. Because of this rather poor sensitivity other statistical measures such as the number variance and spectral rigidity had to be applied to the data to determine q.

C. Number variance and spectral rigidity

In order to check for long-range correlations between the measured levels we have calculated Σ^2 as well as Δ_3 statistics, two measures originally introduced by Dyson and Mehta [16,17] for studies in equivalent fluctuations of nuclear spectra. In this case one is interested in spectral correlations on a scale that contains L mean level spacings. Here

$$\Sigma^2(L) := \langle [n(L) - \langle n(L) \rangle]^2 \rangle = \langle n^2(L) \rangle - L^2 \quad (14)$$

represents the averaged variance of a number $n(L)$ of levels belonging to an interval of length L on the unfolded axis with mean $\langle n(L) \rangle = L$. The quantity $\Delta_3(L)$ is a smoothed and rescaled version of $\Sigma^2(L)$ and can be calculated from

$$\Delta_3(L) = \frac{2}{L^4}\int_0^L dr (L^3 - 2L^2 r + r^3)\Sigma^2(r). \quad (15)$$

Figure 5 shows the experimental results for these two measures as well as the fitted curve according to Berry and Robnik [33] deduced from

$$\Sigma^2_{4,4}(L,q) = \Sigma^2_{\mathrm{Poisson}}((1-q)L) + 4\Sigma^2_{\mathrm{GOE}}\left(q\frac{L}{4}\right), \quad (16)$$

where $\Sigma^2_{\text{Poisson}}$ and Σ^2_{GOE} are the distributions for the pure cases and one symmetry class. An equivalent formula is valid for $\Delta_3(L)$. As in the case of the nearest-neighbor spacing distribution the superposition of four pure Poissonians yields one single Poissonian, which can be directly seen from the analytical expression

$$\Sigma^2_{\text{Poisson}}(L)=L. \tag{17}$$

Inspecting Fig. 5, two results have to be noted. First, the experimental number variance Σ^2 lies clearly between the limiting curves of pure Poissonian and Gaussian characteristics. A fit of the expression (16) to the data yields a mixing parameter of $\Sigma^2(L)$, $q=0.30\pm^{0.20}_{0.30}$ which agrees within the given error range with to the q-value derived from the cumulative nearest-neighbor spacing distribution. On the other hand, the $\Delta_3(L)$ curve corresponds only within the given error range of the data with this result, i.e., a deviation from pure Poissonian behavior is basically not visible. Second, the number variance $\Sigma^2(L)$ clearly displays saturation above a certain value $L_{\max}$. In fact, Berry showed [34] that a global and universal semiclassical (or ray-optical) behavior can only be expected between $L_{\min}=1$ and the value $L_{\max}$, which is determined, on the one hand, by the finite ensemble of resonances, but above all by the lengths of the shortest periodic orbits of the classical system. From Fig. 5 we find $L_{\max}\approx 10$ for Σ^2. Note that $L_{\max}$ of Δ_3 is well approximated by four times $L_{\max}$ of Σ^2 [see Eq. (15) and [35]]. Using a modification of Berry's expression [34] for the electromagnetic case, $L_{\max}$ of Δ_3 can be related to an average length $l_{\min}$ of the shortest periodic orbits via the expression

$$L_{\max}=\frac{3c_0}{l_{\min}f_{\max}}\frac{N_0}{2}, \tag{18}$$

where N_0 is equal to the first term $V_1 f^3$ in Eq. (11) and $f_{\max}$ denotes the upper frequency, i.e., $f_{\max}=20$ GHz. The result is $l_{\min}\approx 0.17$ m, in fair agreement with a value deduced independently in Sec. III E below.

In addition to $\Sigma^2(L)$ and $\Delta_3(L)$ we have also calculated another long-range statistics: the two-level form factor $b_2(t)$ in the corresponding time domain [35,36], which leads to a so-called autocorrelation hole in the case of a GOE-like sequence. It turns out that the fluctuations in b_2 due to the small number of resonances are too large for a proper conclusion and even in the pure GOE case the hole is not very pronounced due to the superposition of symmetry classes.

To summarize the statistical investigation, only the cumulative nearest-neighbor spacing distribution $I(s)$ and the number variance Σ^2 lead to a significant deviation from pure Poissonian behavior for the given set of resonances. Furthermore, the extracted mixing parameter q represents an upper limit for the chaoticity since the assumption of a superposition of four symmetry classes in the statistical analysis increases the weight of the pure GOE contribution with respect to the desymmetrized case.

D. Classical surface of section

In order to obtain an independent estimate for the degree of chaoticity in the system we have also performed a numerical simulation of classical motion inside the 3D cup. Following an idea of Zaslavsky and Strauss [37], we have approximated the resonator's geometry by one-half of a so-called barrel billiard, which can be obtained by cutting a three-axial ellipsoid in two different heights perpendicular to the longest of its axis, see also Fig. 1. Consequently, the surface of the barrel can be described by the curve

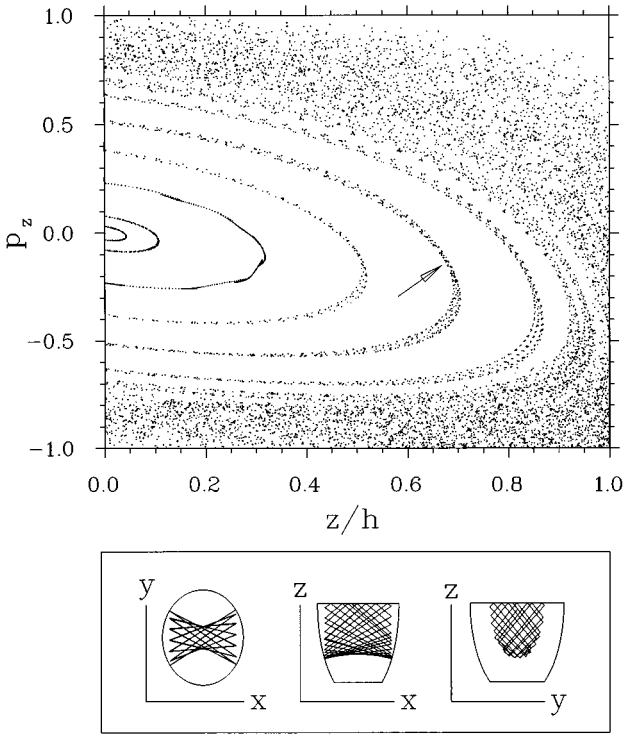

FIG. 6. Poincaré surface of section for the classical barrel billiard. The figure shows the resulting patterns for the conjugated variables (z,p_z) after 16 000 collisions with the boundary. Note that the momentum $|\vec{p}|$ is normalized to unity. As can be seen, the phase space is split in regular stripes and a chaotic sea. The former are produced by a special class of stable orbits, one of which is shown in projections in the lower box of the figure, producing one certain strip pointed out by an arrow. These orbits do not hit the bottom of the cup, thus they only ''see'' the regular ellipsoid.

$$\frac{x^2}{a^2}+\frac{y^2}{b^2}+\frac{z^2}{c^2}=1 \text{ with } z\in[-h,0] \tag{19}$$

and the resonator was modeled with axes $a=58.5/2$ mm, $b=67.6/2$ mm, and cuts at $z=0$ and $z=-h=-56.1$ mm. With respect to these parameters the relative geometrical difference in the volume between the cup resonator and the barrel billiard is about 11%.

To characterize the classical motion of a particle inside this ''half of a barrel geometry'' a two-dimensional area preserving mapping also introduced in [37] was used for creating the underlying Poincaré surface of section. The base of this mapping is simply a pair of a coordinate and its conjugated momentum (z,p_z) of the particle during each reflection on the wall. Note that the momentum $|\vec{p}|$ is normalized to unity. Figure 6 shows the resulting patterns in phase space after 16 000 collisions with the boundary. Because the full ellipsoid is totally regular [38] there exists a class of trajec-

tories (also shown in Fig. 6) manifested by regular stripes on the surface of section that indicate remaining regularities inside the cup. This is due to the fact that these trajectories do not impact on the plane at $z=-h$, which exactly is the reason for overfocusing features of the geometry and consequently the origin of chaos. The relative area of the chaotic part of phase space, the so-called chaotic sea, was estimated by an invariant chaotic Liouville measure of $q\approx 45\%$ using a drastically increased number of about 2×10^5 wall collisions to get a higher accuracy. This is larger than the mixing parameter deduced from $I(s)$ and Σ^2, but it has to be noted that the applicability of the Berry-Robnik model was originally shown to depend strongly upon reaching the semiclassical (or ray-optical) limit, which in the two-dimensional case is established only far beyond thousands of eigenvalues [39]. The present case of only close to 300 eigenvalues at least points to the correct tendency for the correspondence between the classical Liouville measure and the wave dynamical mixing parameter extracted from the data.

E. Periodic orbit theory

As a final study of semiclassical features of our wave dynamical system, we have analyzed the spectrum of classical orbit length l in the 3D cup, which is directly related to the measured frequency spectrum by a Fourier transform of the above mentioned fluctuating part of the eigenmode density [Eq. (7)],

$$\widetilde{\rho}^{\mathrm{fluc}}(l)=\int_{f_{\min}}^{f_{\max}}\rho^{\mathrm{fluc}}(f)\exp\left(i\frac{2\pi}{c_0}lf\right)df$$
$$=\int_{f_{\min}}^{f_{\max}}[\rho(f)-\rho^{\mathrm{smooth}}(f)]\exp\left(i\frac{2\pi}{c_0}lf\right)df. \tag{20}$$

Here $f_{\min}$ and $f_{\max}$ denote the borders of the measured frequency range, i.e., 0 and 20 GHz. Figure 7 shows in the upper part the value $|\widetilde{\rho}^{\mathrm{fluc}}(l)|^2$ in a range of orbit lengths l up to 0.5 m and in the lower part some periodic orbits obtained from numerical simulations on the barrel billiard are presented. As can be seen from the arrows below the abscissa, several of those orbits correspond well to the locations of peaks in the Fourier spectrum of the data. The shortest periodic orbit that bounces between the bottom and the lid has a length of $l=0.1122$ m, which is close to the independent estimate of Sec. III C above. It is the so-called shortest bouncing ball orbit in the cup.

F. 3D bouncing ball orbit

This bouncing ball orbit has been analyzed in a more quantitative manner. Following [40], we have calculated an additional term of the smooth part of the staircase function Eq. (11), attached to the three-dimensional bouncing ball orbit propagating periodically between the bottom and the lid of the cup. Again the contributions for both polarization classes have to be considered separately. The result for the sum of both parts as pointed out in the Appendix is given by

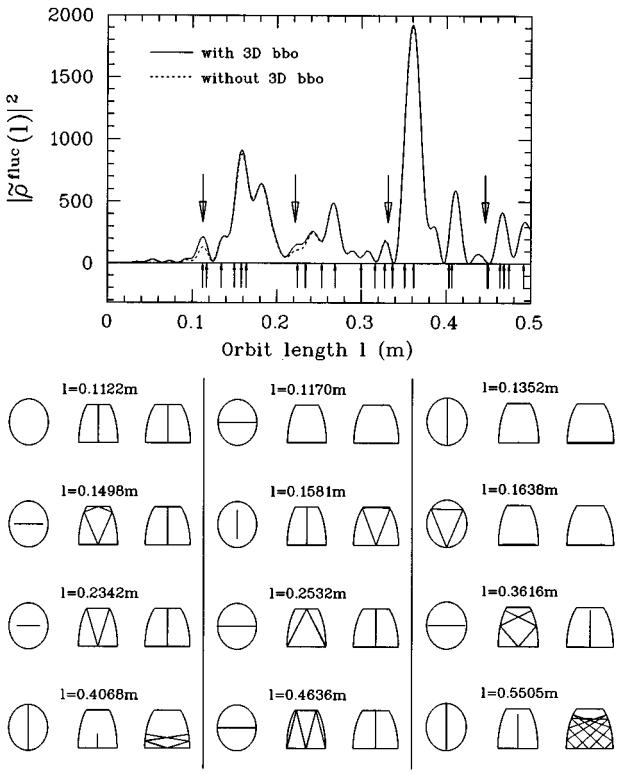

FIG. 7. Length spectrum (upper part) from the Fourier transformed fluctuating part of the eigenmode density of the 3D cup (solid curve) and some numerically simulated periodic orbits for the barrel billiard (lower part). The lengths of these orbits and of their multiples are indicated by arrows below the abscissa for comparison with the experiment. In addition, the contribution of the 3D-bouncing ball orbit with $l_{\mathrm{BBO}}=0.1122$ m has been extracted from the spectrum (dashed curve). The larger arrows above the curve indicate multiples of l_{BBO} to guide the eye.

$$N_{\mathrm{em}}^{\mathrm{BBO}}(X)=N_{\mathrm{TM}}^{\mathrm{BBO}}+N_{\mathrm{TE}}^{\mathrm{BBO}}$$
$$=\frac{\pi S}{2h^2}\left(\sum_{0<n<X}(X^2-n^2)-\frac{2}{3}X^3+\frac{1}{2}X^2\right), \tag{21}$$

where $X=kh/\pi=2hf/c_0$ and $h=56.1$ mm, half of the bouncing ball orbit's length, i.e., the heigth of the cup. The parameter S denotes the area on which this orbit exists, i.e., the size of the cup's bottom. The upper part of Fig. 7 also shows the result for the remaining length spectrum after extracting this contribution. In fact, the peak belonging to the correct length of the bouncing ball orbit does not vanish completely because it is due to a superposition of two adjacent periodic orbits, the bouncing ball orbit at $l=0.1122$ m and a stable periodic orbit at $l=0.1170$ m, as seen from the lower part of Fig. 7.

In order to verify the new electromagnetic bouncing ball formula (21), independently from this result we also have tested it using a set of $\approx 20\,000$ eigenmodes of a regular box. This system is classically integrable, thus it is possible to calculate the electromagnetic eigenfrequencies analytically. The box also allows to study the different polarizations, TE and TM modes, in more detail and especially their system-

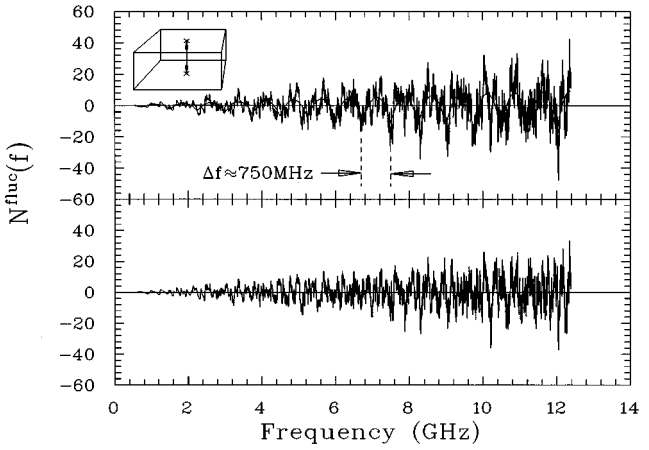

FIG. 8. Fluctuating part of the staircase function for a regular box using the first 20 000 eigenfrequencies. In the upper part an impressive oscillation, with period $\Delta f \approx 750$ MHz, which is due to the contribution of the shortest 3D-bouncing ball orbit (shown in the inset), can be observed. The theoretical investigation [Eq. (21)] resulted in the smooth curve also superimposed in the upper part of the figure. After the extraction of this bouncing ball contribution the oscillations around zero revealed a lower magnitude and the corresponding period Δf vanished from the fluctuations (lower part).

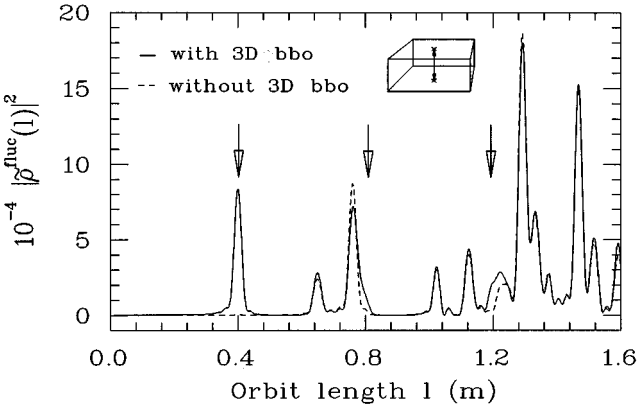

FIG. 9. Length spectrum for the regular box in a range between 0 and 1.6 m (solid curve). In this presentation the discussed bouncing ball orbit leads to an impressive peak at $l_{\mathrm{BBO}}=0.4$ m. The positions of its multiples are denoted by arrows in the figure. Again the contribution of this orbit has been extracted and now the remaining spectrum (dashed curve) can be seen to be free of any remnant.

atic degeneration, which directly follows from the analytical expression for the eigenfrequencies

$$f_{u,v,w}=\frac{c_0}{2}\sqrt{\left(\frac{u}{A}\right)^2+\left(\frac{v}{B}\right)^2+\left(\frac{w}{C}\right)^2} \tag{22}$$

with

$$u,v=1,2,3,\ldots;\quad w=0,1,2,\ldots \quad \text{for TM}$$

$$u,v=0(\text{ either } u \text{ or } v),1,2,\ldots;\quad w=1,2,3,\ldots \quad \text{for TE.}$$

In order to avoid further accidental number theoretical degeneracies the lengths of the three edges A, B, and C were chosen as $A=0.2$ m, $B=\gamma A$, and $C=\gamma^2 A$, where $1/\gamma=(\sqrt{5}-1)/2$, the ratio of the golden mean. Following Eq. (6) we have calculated the exact smooth part of the staircase function for the given set of eigenfrequencies. Here the linear term and the constant term are given analytically without any free parameter. Extracting this smooth part from the total staircase of the box [Eq. (9)], we obtained the fluctuating part, which is shown in the upper part of Fig. 8. The present choice of the edges A, B, and C yields a very clear oscillation in this fluctuating part, which is dominated by one certain classical bouncing ball orbit (also given in Fig. 8). The length of this orbit l_{BBO} corresponds to the period of the observed oscillation $\Delta f=c_0/l_{\mathrm{BBO}}=c_0/2A\approx 750$ MHz. Using the area $S_{\mathrm{BBO}}=BC$ for this certain orbit, we have calculated the contribution that follows from Eq. (21). This curve is also represented in the upper part of Fig. 8 and reproduces the data very well as it can be seen in the lower part of the same figure where the bouncing ball contribution has been extracted from the staircase function, i.e., where the modulation of Δf is not present anymore. Note that the impressive amplitude of the given modulation is due to the ratio $2\pi S_{\mathrm{BBO}}/l_{\mathrm{BBO}}^2=(\pi/2)\gamma^3\approx 6.65$ in Eq. (21), which is the largest contribution in comparison to the other possible bouncing ball orbits and also much larger than the corresponding amplitude for the 3D cup, $\pi S/(2h^2)\approx 0.45$.

To perform a more obvious test of Eq. (21) we again have calculated the Fourier spectrum, Eq. (20), of the calculated set of eigenfrequencies. The result is shown in Fig. 9. The bouncing ball orbit leads to an impressive peak at a length $l_{\mathrm{BBO}}=0.4$ m. Using Eq. (21) in the same way, i.e., calculating the Fourier transformed of $N_{\mathrm{em}}^{\mathrm{BBO}}$ we are able to extract this peak without any remnant as well as contributions of its multiples, which indicates that the orbit has been described correctly by Eq. (21). Because of this result, which was achieved successfully for several boxes of different proportions, we are certain that the remaining peak in the length spectrum of the 3D cup in Fig. 7 is due to the existence of the stable periodic orbit of 0.1170 m length.

As an additional test of statistical measures, we have calculated the nearest-neighbor spacing distribution and the

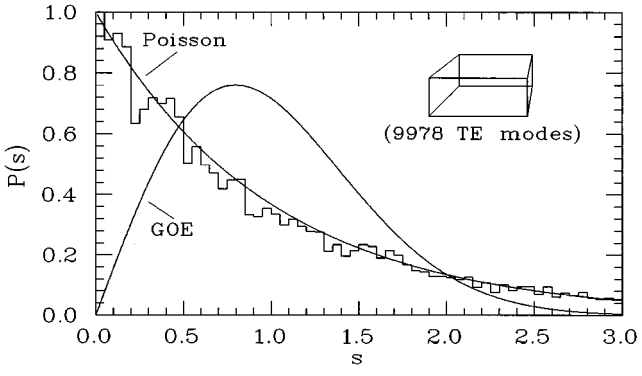

FIG. 10. Nearest-neighbor spacing distribution for the regular box. Because of the systematic degeneration of almost all TE and TM modes, the calculation was restricted to one polarization (9978 TE modes). Due to the fact that the system is desymmetrized by definition, the limiting curve for the chaotic case is given by a single GOE distribution. As expected, for the regular box the system shows pure Poissonian characteristics.

Σ^2 and the Δ_3 statistics for both polarizations of the box separately. This yields pure Poissonian characteristics across the whole range of spacings as expected for the given regular system. As an example, the result for the nearest-neighbor spacing distribution using the first 9978 TE modes is presented in Fig. 10.

Returning to the 3D cup, for completion we have calculated the statistical measures of the short- and long-range correlations after extraction of the bouncing ball contribution, i.e., we have reunfolded the experimental spectrum in adding Eq. (21) to the standard Weylian Eq. (11) and repeated our statistical analysis. The effect is rather weak, as can be expected because of the small amplitude of Eq. (21) in the case of the cup. The procedure leads to a very slight correction of the Σ^2 and the Δ_3 curves towards the pure GOE limit, but its influence on the mixing parameter is much smaller than the quoted uncertainties.

IV. CONCLUSION

In summary, we have applied several original quantum methods such as eigenvalue statistics and periodic orbits in the given case of a purely classical, vectorial wave phenomenon. Although the spectrum was checked for completeness using the correct electromagnetic Weyl formula Eq. (11), the fluctuations around this mean behavior are not very sensitive for the details of the boundary in the present case of only 286 resonances. On the other hand, the system was analyzed in terms of periodic orbit theory. As the length spectrum of the resonator leads to more detailed conclusions (estimations for the saturation of Σ^2 and Δ_3 via the shortest periodic orbits, identification of classicals orbit lengths, and extraction of the first bouncing ball orbit) this analysis proves to be a helpful tool for investigations in the near semiclassical limit. Comparing the classical degree of chaoticity ($q_{\mathrm{cl}} \approx 0.45$) with the corresponding mixing parameter deduced from spectral statistics according to the model of Berry and Robnik, only the cumulative nearest-neighbor spacing distribution $I(s)$ and the number variance Σ^2 significantly deviate from the pure Poissonian behavior and show the correct tendency ($q > 0$). The uncertainties of the analysis are not due to fundamental difficulties but rather a consequence of the poor desymmetrization and the small size of the cup, yielding only 286 resonances in the accessible frequency range. Therefore, in order to study the ''three-dimensional Helmholtz chaos'' in a more quantitative and proper way we have already started measurements on a precisely manufactured, fully desymmetrized 3D Sinai billiard realized by 1/48 of a cube with a centered sphere [26]. Besides testing the usual statistical measures, we will especially investigate the ray-optical generalization of Gutzwiller's quantum trace formula following the very advanced ideas of Balian and Duplantier [32].

ACKNOWLEDGEMENTS

We would like to thank F. Neumeyer and S. Strauch for helpful advice concerning the numerical calculations and our mechanical workshop for the excellent fabrication of the niobium resonator. This work has been supported by the Sonderforschungsbereich 185 ''Nichtlineare Dynamik'' of the Deutsche Forschungsgemeinschaft, in part by the Bundesministerium für Bildung und Forschung under Contract No. 06DA665I, and through a Max-Planck-Forschungspreis.

APPENDIX: THE BOUNCING BALL STAIRCASE FUNCTION IN *D* DIMENSIONS

First, we construct the general contribution of a bouncing ball orbit in a D-dimensional cavity ($D > 1$) to the spectral staircase function of nonrelativistic quantum mechanics, $N_D^{\mathrm{BBO}}(k)$ with $k = 2\pi f/c_0$, and second we apply these general results to the electromagnetic case in $D = 3$ dimensions. As usual, the spectral staircase function is given as the integral over the spectral density $\rho_D^{\mathrm{BBO}}(E)$,

$$N_D^{\mathrm{BBO}}(k) = \int_0^k d\tilde{k}\,\rho_D^{\mathrm{BBO}}(\tilde{k}) = \int_0^k d\tilde{k}\frac{d\tilde{E}}{d\tilde{k}}\rho_D^{\mathrm{BBO}}(\tilde{E}) = \int_0^k d\tilde{k}\frac{\hbar^2\tilde{k}}{m}\rho_D^{\mathrm{BBO}}(\tilde{E}), \tag{A1}$$

where m is the mass of the nonrelativistic particle inside the cavity. The spectral density in turn is given by the imaginary part of the trace of the nonrelativistic Green's function inside the cavity

$$\rho_D^{\mathrm{BBO}}(E) = -\lim_{\epsilon\to 0}\frac{1}{\pi}\mathrm{Im}\,\mathrm{Tr}[G(E+i\epsilon)] = -\lim_{\epsilon\to 0}\frac{1}{\pi}\mathrm{Im}\sum_{n(\geqslant)0}^{>}\frac{S_\perp^{(D-1)}}{(2\pi)^{D-1}} \times \int d^{D-1}k_\perp \frac{1}{E+i\epsilon-\frac{\hbar^2}{2m}\left(k_\perp^2+\frac{n^2\pi^2}{l^2}\right)}. \tag{A2}$$

Here l is half of the total length of the bouncing ball orbit and $S_\perp^{(D-1)}$ is the size of the smallest of the two parallel (D-1)-dimensional ''surfaces'' between which the orbit bounces. The integer n labels the modes along the bouncing ball orbit with $n > 0$ or $n \geqslant 0$ for Dirichlet or Neumann boundary conditions on the two surfaces, respectively. The momentum component along the orbit is $n\pi/l$. The $(D-1)$-dimensional momentum integration perpendicular to the bouncing ball orbit is the free unrestricted one. The factors in front of the integral are the phase space normalization factors in D-1 dimensions. After the insertion of Eq. (A2) into Eq. (A1), the spectral staircase function reads

$$N_D^{\mathrm{BBO}}(k) = \int_0^{k^2} d(\tilde{k}^2)\frac{S_\perp^{(D-1)}}{(2\pi)^{D-1}}\sum_{n(\geqslant)0}^{>}\int d\Omega_{k_\perp}^{(D-1)} \times \int_0^\infty dk_\perp k_\perp^{D-2}\delta\left(k_\perp^2+\frac{n^2\pi^2}{l^2}-\tilde{k}^2\right), \tag{A3}$$

where $\int d\Omega_{k_\perp}^{(D-1)} = 2\pi^{(D-1)/2}/\Gamma((D-1)/2)$ is the angular integral in D-1 dimensions. In writing down Eq. (A3) we used the relation $\lim_{\epsilon\to 0}\mathrm{Im}(x-x_0-i\epsilon)/\pi = \delta(x-x_0)$. Now the integrations in Eq. (A3) become simple because of the δ function. The final result for the bouncing ball orbit of a nonrelativisitic particle inside a cavity in $D>1$ dimensions is therefore

$$N_D^{\mathrm{BBO}}(k) = \frac{S_\perp^{(D-1)}}{\Gamma\left(\frac{D-1}{2}\right)(2\sqrt{\pi})^{D-1}}\frac{1}{\frac{D-3}{2}+1} \times \sum_{0\,(\leqslant)\,n<kl/\pi}\left(k^2-\frac{n^2\pi^2}{l^2}\right)^{(D-3)/2+1}. \quad \text{(A4)}$$

This formula applied to two dimensions reads

$$N_2^{\mathrm{BBO}}(k) = \frac{L}{\pi}\sum_{0\,(\leqslant)\,n<kl/\pi}\sqrt{k^2-\frac{n^2\pi^2}{l^2}}, \quad \text{(A5)}$$

where $L = S_\perp^{(1)}$ is the length perpendicular to the bouncing ball orbit. It agrees of course with the result of Ref. [40]. The three-dimensional expression has the form

$$N_3^{\mathrm{BBO}}(k) = \frac{S}{4\pi}\sum_{0\,(\leqslant)\,n<kl/\pi}\left(k^2-\frac{n^2\pi^2}{l^2}\right), \quad \text{(A6)}$$

where $S = S_\perp^{(2)}$ denotes the plane perpendicular to the bouncing ball orbit. The bouncing ball contribution in three dimensions to the *fluctuating* part of the spectral staircase function is now given by formula (A6) minus its contribution to the Weyl or smooth part of the spectral staircase function, which has to be subtracted in order to avoid double counting. The smooth part follows from Eq. (A6) via the application of the Euler-MacLaurin formula $\frac{1}{2}F(0)+F(1)+F(2)+\cdots F(N-1)+\frac{1}{2}F(N) = \int_0^N dx F(x)+\cdots$, where $F(x)\propto(k^2-x^2\pi^2/l^2)$ and the ellipsis corresponds to the fluctuating contribution here. Thus we have

$$N_3^{\mathrm{BBO,smooth}}(k) = \frac{S}{4\pi}\left[\int_0^{kl/\pi}dx\left(k^2-\frac{x^2\pi^2}{l^2}\right)\mp\frac{1}{2}k^2\right] = \frac{Slk^3}{6\pi^2}\mp\frac{Sk^2}{8\pi}, \quad \text{(A7)}$$

where the last term takes into account the factor 1/2 in front of the first term $F(0)$ in the Euler-MacLaurin formula and the extra mode in the Neumann case. We do not get an extra contribution from the upper boundary, as $F(N)$ vanishes in the average in our case. In summary, in nonrelativistic quantum mechanics, the bouncing ball contribution to the fluctuating part of the spectral staircase function in a three-dimensional cavity reads

$$N_3^{\mathrm{BBO,\,fluc}}(k) = \frac{S}{4\pi}\sum_{0\,(\leqslant)\,n<\frac{kl}{\pi}}\left(k^2-\frac{n^2\pi^2}{l^2}\right)-\frac{Slk^3}{6\pi^2}\pm\frac{Sk^2}{8\pi}, \quad \text{(A8)}$$

where the upper signs and inequalities apply to Dirichlet boundary conditions on the two surfaces between which the orbit bounces, whereas the lower signs and inequalities refer to the Neumann case. In the electromagnetic case these two contributions correspond to the magnetic and electric bouncing ball modes, respectively [see Eq. (5)], which decouple for modes along the bouncing ball orbit. Therefore we can just sum both terms to get the final expression for the bouncing ball contribution to the fluctuating part of the staircase function for an electromagnetic cavity in three dimensions:

$$N_{\mathrm{em}}^{\mathrm{BBO,\,fluc}}(X) = \frac{\pi S}{2l^2}\left(\sum_{0<n<X}(X^2-n^2)-\frac{2}{3}X^3+\frac{1}{2}X^2\right), \quad \text{(A9)}$$

with $X = kl/\pi$.

[1] G.D. Birkhoff, Acta Math. **50**, 359 (1927).
[2] L.A. Bunimovich, Zh. Éksp. Teor. Fiz. **89**, 1452 (1985) [Sov. Phys. JETP **62**, 842 (1985)].
[3] Ya. G. Sinai, Sov. Math. Dokl. **4**, 1818 (1963).
[4] S.W. McDonald and A.N. Kaufman, Phys. Rev. Lett. **42**, 1189 (1979).
[5] O. Bohigas, in *Chaos and Quantum Physics*, edited by M.-J. Giannoni, A. Voros, and J. Zinn-Justin (Elsevier, Amsterdam, 1991), p. 89.
[6] F. Steiner, in *Schlaglichter der Forschung, Zum 75. Jahrestag der Universität Hamburg 1994*, edited by R. Ansorge (Reimer, Berlin, 1994), p. 543.
[7] M.C. Gutzwiller, *Chaos in Classical and Quantum Mechanics* (Springer, New York, 1990).
[8] M.V. Berry, Proc. R. Soc. London Ser. A **413**, 183 (1987).
[9] H.-J. Stöckmann and J. Stein, Phys. Rev. Lett. **64**, 2215 (1990).
[10] J. Stein and H.-J. Stöckmann, Phys. Rev. Lett. **68**, 2867 (1992).
[11] S. Sridhar, Phys. Rev. Lett. **67**, 785 (1991).
[12] H.-D. Gräf, H.L. Harney, H. Lengeler, C.H. Lewenkopf, C. Rangacharyulu, A. Richter, P. Schardt, and H.A. Weidenmüller, Phys. Rev. Lett. **69**, 1296 (1992).
[13] H. Alt, P. von Brentano, H.-D. Gräf, R.-D. Herzberg, M. Philipp, A. Richter, and P. Schardt, Nucl. Phys. A **560**, 293 (1993).
[14] H. Alt, H.-D. Gräf, H.L. Harney, R. Hofferbert, H. Lengeler, C. Rangacharyulu, A. Richter, and P. Schardt, Phys. Rev. E **50**, 1 (1994).
[15] H. Alt, H.-D. Gräf, H.L. Harney, R. Hofferbert, H. Lengeler, A. Richter, P. Schardt, and H.A. Weidenmüller, Phys. Rev. Lett. **74**, 62 (1995).
[16] F.J. Dyson and M.L. Mehta, J. Math. Phys. **4**, 701 (1963).
[17] M.L. Mehta, *Random Matrices and the Statistical Theories of Energy Levels* (Academic, New York, 1967).
[18] O. Bohigas, M.J. Giannoni, and C. Schmit, Phys. Rev. Lett. **52**, 1 (1984).
[19] M.V. Berry and M. Tabor, Proc. R. Soc. London Ser. A **356**, 375 (1977).

[20] J.D. Jackson, *Classical Electrodynamics*, 2nd ed. (Wiley, New York, 1975).
[21] M.R. Schröder, Acustica **4**, 456 (1954); [reprinted in J. Audio Eng. Soc. **35**, 307 (1987)].
[22] R.L. Weaver, J. Acoust. Soc. Am. **85**, 1005 (1989).
[23] C. Ellegaard, T. Guhr, K. Lindemann, H.Q. Lorensen, J. Nygård, and M. Oxborrow, Phys. Rev. Lett. **75**, 1546 (1995).
[24] S. Deus, P.M. Koch, and L. Sirko, Phys. Rev. E **52**, 1146 (1995).
[25] R. Balian and C. Bloch, Ann. Phys. (N.Y.) **64**, 271 (1971).
[26] H. Primack and U. Smilansky, Phys. Rev. Lett. **74**, 4831 (1995).
[27] O. Frank and B. Eckhardt, Phys. Rev. E **53**, 4166 (1996).
[28] J. Auerhammer, H. Genz, H.-D. Gräf, R. Hahn, P. Hoffmann-Stascheck, C. Lüttge, U. Nething, K. Rühl, A. Richter, T. Rietdorf, P. Schardt, E. Spamer, F. Thomas, O. Titze, J. Töpper, and H. Weise, Nucl. Phys. A **553**, 841c (1993).
[29] H. Weyl, J. Reine Angew. Math. Band **141**, 1 (1912); **141**, 163 (1912).
[30] H. Weyl, J. Reine Angew. Math. Band **143**, 177 (1913).
[31] H.P. Baltes and E.R. Hilf, *Spectra of Finite Systems* (Bibliographisches Institut, Mannheim, 1975).
[32] R. Balian and B. Duplantier, Ann. Phys. (N.Y.) **104**, 300 (1977).
[33] M.V. Berry and M. Robnik, J. Phys. A **17**, 2413 (1984).
[34] M.V. Berry, Proc. R. Soc. London Ser. A **400**, 229 (1985).
[35] A. Delon, R. Jost, and M. Lombardi, J. Chem. Phys. **95**, 5701 (1991).
[36] M. Lombardi, O. Bohigas, and T.H. Seligman, Phys. Lett. B **324**, 263 (1994).
[37] G. Zaslavsky and H.R. Strauss, in *Irregular Atomic Systems and Quantum Chaos*, edited by J.C. Gay (Gordon and Breach, Philadelphia, 1992), p. 51.
[38] M.V. Berry, Eur. J. Phys. **2**, 91 (1981).
[39] M. Robnik, J. Phys. Soc. Jpn. Suppl. A **63**, 131 (1994).
[40] M. Sieber, U. Smilansky, S.C. Creagh, and R.G. Littlejohn, J. Phys. A **26**, 6217 (1993).